PHARMACON
Jurnal Farmasi Indonesia
Pharmaceutical Journal of Indonesia

Pharmacon: Jurnal Farmasi Indonesia
Vol. 23, No. 1 (2026), pp. 112–121
DOI:10.23917/pharmacon.v23i1.16383
p-ISSN: **1411-4283**, e-ISSN: **2685-5062**

Shallot Leaf Extract-Loaded Nanostructured Lipid Carrier as a Preliminary Platform for STMN1-Targeted Screening and Macrophage Phagocytic Activity Enhancement

Amna Falistina[1], Bilqis Alfisyahani[2], Yuda Faturohman[3*], Adyatma Riyandino[4], Anantazea Deniss Kumara[5], Talitha Widiatningrum[6]

[1,2 6] Biology, Faculty of Mathematics and Natural Sciences, Universitas Negeri Semarang, Indonesia
[3,4] Chemistry Education, Faculty of Mathematics and Natural Sciences, Universitas Negeri Semarang, Indonesia
[5] Pharmacy Studi Program, Faculty of Medicine, Universitas Negeri Semarang, Indonesia
**Corresponding author: yudafaturohman@students.unnes.ac.id*

ARTICLE HISTORY:
Submitted : 2026-02-23
Accepted. : 2026-06-25
Published : 2026-06-30

KEYWORDS:
Lipid carriers; Macrophage phagocytosis; Molecular docking; Nanostructured; Shallot leaf extract; STMN1

Citation:
Falistina, A., Alfisyahani, B., Faturohman, Y., Riyandino, A., Kumara, A.D., Widiatningrum, T. (2026). Shallot Leaf Extract-Loaded Nanostructured Lipid Carrier as a Preliminary Platform for STMN1-Targeted Screening and Macrophage Phagocytic Activity Enhancement. Pharmacon: Jurnal Farmasi Indonesia, 23(1), 112-121. https://doi.org/10.23917/pharmacon.v23i1.16383

ABSTRACT

Cancer metastasis remains a major therapeutic challenge involving molecular dysregulation and tumor–microenvironment interactions. Stathmin 1 (STMN1), a microtubule-destabilizing regulator related to cell motility and tumor aggressiveness, is relevant for preliminary anti-metastasis-oriented screening. Nanostructured lipid carriers (NLC) may improve the dispersion and delivery performance of natural-product extracts. This study formulated shallot leaf (*Allium cepa* L.) extract into an NLC dispersion using emulsification–ultrasonication under homogenized and non-homogenized conditions, followed by PSA/DLS and SEM characterization. Phytochemical candidates curated from databases and literature were docked to STMN1 to identify ligands with favorable predicted binding profiles. Macrophage phagocytic function was evaluated using a latex-bead assay at 0, 5, and 10 µL. PSA/DLS and SEM indicated particulate structures, but particle-size variation and aggregation suggested the need for further formulation optimization and stability evaluation. Docking ranked sinapic acid (−7.5 kcal/mol) and ferulic acid (−7.4 kcal/mol) as the best phenolic candidates among the tested ligands, although the GDP control showed stronger predicted affinity. Phagocytic capacity increased from 33.5% (0 µL) to 37% (5 µL) and 91% (10 µL), while the phagocytic index increased from 0.63 to 0.77 and 4.50, respectively. The 10 µL dose was the most responsive condition for enhancing macrophage phagocytic activity. These findings should be interpreted as preliminary evidence of STMN1-oriented in silico prioritization and macrophage functional enhancement, not direct proof of anti-metastatic activity or M2 macrophage inhibition.

INTRODUCTION

Cancer is a disease characterized by uncontrolled proliferation of abnormal cells that can invade surrounding tissues and spread to distant organs through metastasis. Global estimates from GLOBOCAN 2022 report nearly 20 million new cancer cases and approximately 9.7 million deaths, indicating that the need for therapeutic innovation remains high worldwide (Bray et al., 2024). Metastasis represents a critical challenge because it is strongly associated with treatment failure at advanced stages and with poorer clinical outcomes (Zeng et al., 2024). Microtubule dynamics play an essential role in cell migration, making stathmin 1 (STMN1), a microtubule-destabilizing regulator, frequently associated with tumor aggressiveness and metastatic behavior. Recent evidence indicates that STMN1 can contribute to metastasis through microtubule-related mechanisms and has therefore been considered a potential molecular target for anti-metastatic intervention (Liu et al., 2023). The tumor

microenvironment is also shaped by innate immune cells, particularly macrophages, which can "partner" with tumor cells to promote directed migration and support metastatic progression(Friedman-DeLuca et al., 2024).

Recent advances in topical drug delivery have positioned Nanostructured Lipid Carriers (NLC) as lipid-based nanocarriers capable of improving loading capacity, stability, and sustained release (Kumari et al., 2026). Incorporation of NLC into hydrogel matrices has been reported to enhance application comfort, prolong local residence time, and improve drug retention within skin layers (Calderon-Jacinto et al., 2022). Natural-product research on the genus *Allium* has highlighted the presence of flavonoids and organosulfur compounds with potential anticancer activity through diverse biological mechanisms (Imran et al., 2020; Iwar et al., 2024). The resulting gap creates an opportunity to integrate an *Allium*-based NLC–gel platform with mechanistic evaluation connecting STMN1 targeting and macrophage responses as key components of the metastatic microenvironment (Friedman-DeLuca et al., 2024).

This study offers novelty through the development of a shallot leaf extract-loaded NLC dispersion and its evaluation using a staged evidentiary workflow spanning formulation, in silico target exploration, and macrophage functional assessment. The study aims to formulate an NLC system containing shallot leaf extract and incorporate it into a gel base to enhance stability and topical performance. Additional objectives include characterization of product quality, including particle size, PDI, zeta potential, morphology, and gel-related parameters required to establish formulation feasibility (Calderon-Jacinto et al., 2022). Mechanistic objectives focus on identifying selected compounds from the extract and evaluating their predicted binding affinity toward STMN1, a target associated with migration and metastasis in specific cancer contexts (Liu et al., 2023). Biological objectives focus on testing macrophage responses using a functional phagocytosis assay to capture early trends in innate immune modulation, without directly claiming macrophage polarization or M2 inhibition in the absence of marker-based evidence (Friedman-DeLuca et al., 2024).

METHODS

Formulation of Shallot-Leaf NLC Nanoparticles

Plant Material Preparation and Maceration Extraction

Shallot leaves (*Allium cepa* L.) were washed, drained, dried, and milled into fine simplisia powder. The powdered simplisia (300 g) was macerated with 96% technical ethanol (1.8 L) for 3 × 24 h at room temperature with occasional stirring. The filtrate was collected and concentrated by solvent evaporation to obtain a viscous crude extract (Krakowska-Sieprawska et al., 2022).

Preparation of nanostructured lipid carriers (NLC) by emulsification–ultrasonication

Nanostructured lipid carriers (NLC) were prepared using an emulsification–ultrasonication approach adapted from published NLC preparation methods (Elkhateeb et al., 2023). Oil phase consisted of shallot leaf extract (0.5 mL), glyceryl monostearate (7 mL), capric acid (3 mL), and lecithin (5 mL). Aqueous phase consisted of Tween 80 (2 mL) and ultrapure water (67.5 mL). Oil and aqueous phases were heated separately to 70 °C, then the aqueous phase was added dropwise to the oil phase at 70 °C under continuous agitation (8000 rpm). Emulsions were immediately subjected to high-intensity sonication for 10 min followed by cooling to room temperature.

Experimental characterization

Particle size distribution and polydispersity

Particle size and polydispersity index (PDI) were measured using a Particle Size Analyzer (PSA). The NLC dispersion was diluted with distilled water to obtain a 100 ppm colloid, transferred into a cuvette, and analyzed to determine particle size and polydispersity index.

Morphological Characterization of NLC by SEM

Scanning electron microscopy (SEM) was used to observe surface morphology. Sample

preparation and imaging followed the standard SEM workflow available in the hosting facility.

In silico analysis: STMN1 (stathmin) docking

Ligand collection and preparation

Bioactive compounds were compiled from Dr. Duke's Phytochemical and Ethnobotanical Database using the keyword "*Allium cepa*," (Duke, 2016). Ligand structures were retrieved from PubChem in SDF format (Kim et al., 2023).

Protein target preparation (STMN1)

Stathmin (STMN1) was defined as the docking target. A 3D structure model for STMN1 was obtained from the AlphaFold Protein Structure Database (AlphaFold DB) (Varadi et al., 2022). Protein preprocessing included removal of non-essential molecules (e.g., waters) and basic structure cleaning using PyMOL

Molecular docking and interaction analysis

Docking simulations were carried out using AutoDock Vina through the PyRx 0.8 interface (Trott & Olson, 2010). Docking outputs were saved in PDBQT format for downstream visualization and analysis. Binding poses were visualized in PyMOL, and 2D interaction diagrams were generated using LigPlot+ to summarize hydrogen bonding and hydrophobic contacts.

In vitro assay: macrophage phagocytosis using latex beads

Treatment design

Macrophage cultures were prepared following the laboratory's established workflow. NLC formulation was applied at volume-based doses of 0 µL, 5 µL, and 10 µL, with two experimental repeats per condition (as conducted), and incubated for 4 h.

Latex bead challenge, fixation, and staining

Latex bead phagocytosis was used as the functional readout of macrophage activity. After treatment incubation, residual formulation was removed and 200 µL latex bead suspension was added to each culture, followed by 60 min incubation. Uninternalized beads were removed by washing, cells were rinsed with PBS, fixed using methanol, air-dried at room temperature, and stained with 10% Giemsa.

Microscopy and quantification

Light microscopy at 400× magnification was used to quantify phagocytosis by counting (i) the number of macrophages actively phagocytosing per 100 macrophages (phagocytic capacity) and (ii) the number of internalized beads per 100 macrophages (phagocytic index). Data were analyzed using one-way ANOVA at a significance level of $\alpha = 0.05$. When the homogeneity assumption was met, Tukey's HSD was applied for pairwise comparisons. When variances were unequal (heteroscedasticity), the Games–Howell post hoc test was used for multiple comparisons (Pavlova et al., 2023).

RESULT

Preparation of NLC dispersions

Preparation of the NLC dispersions produced two formulations with distinct visual appearances under the non-homogenized and homogenized conditions (Elkhateeb et al., 2023). The non-homogenized dispersion exhibited lower visual uniformity than the homogenized dispersion. The homogenized dispersion appeared more visually uniform than the non-homogenized sample (Kumari et al., 2026).

(a) (b)

Figure 1. Results of NLC gel synthesis: (a) without homogenization; (b) homogenized.

Particle size and polydispersity index

Particle size and dispersity were measured using a Particle Size Analyzer (PSA) operated under the dynamic light scattering (DLS) principle (Hackley & Clogston, 2020). The particle-size profiles differed between the homogenized and non-homogenized preparations.

The homogenized sample showed a small-size peak at 2.3 nm (Figure 2), whereas the non-homogenized sample showed a peak at 33.9 nm (Figure 3). Nevertheless, the 2.3 nm peak was interpreted cautiously because this size is below the typical dimension expected for intact lipid-core NLC particles and may correspond to micellar or surfactant-associated colloidal species. The dispersion also showed a Z-average of 3729.2 nm and a polydispersity index (PDI) of 0.340.

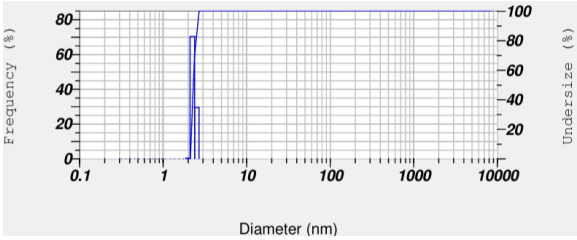

Figure 2. PSA results of homogenized NLCs.

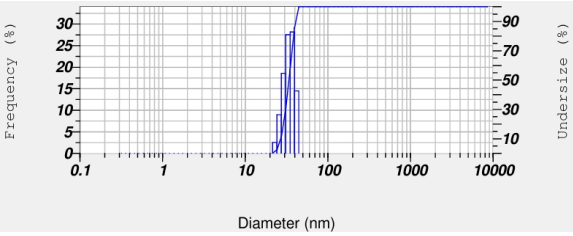

Figure 3. PSA results of non-homogenized NLCs.

Morphological characterization of NLC by SEM

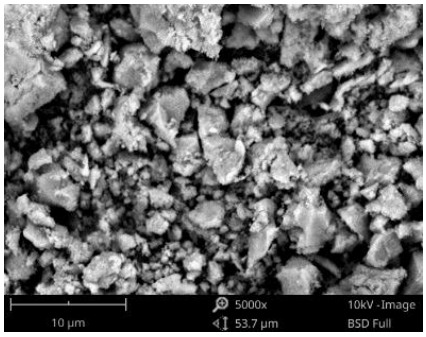

Figure 4. SEM analysis results of NLCs.

Morphological characterization of the prepared NLC dispersions was performed using scanning electron microscopy (SEM). The SEM micrographs revealed particulate structures with irregular morphology and a tendency to form aggregates rather than discrete, uniformly separated spherical nanoparticles (Figure 4).

The presence of particle clusters and uneven surface features suggests that agglomeration may have occurred during sample preparation, drying, or imaging, which is commonly observed in electron microscopy analysis of colloidal lipid-based systems (Bresch et al., 2022). These observations are consistent with the PSA results, which indicated the presence of larger particle populations or aggregates in the dispersion. Therefore, the SEM results support the formation of particulate structures in the prepared dispersion, but they do not yet provide sufficient evidence to confirm a fully uniform and physically stable NLC system. Further optimization of the formulation process and additional stability evaluations, including zeta potential measurement and storage stability testing, are required to confirm colloidal stability and reduce aggregation (Chauhan et al., 2020).

Molecular docking results against STMN1

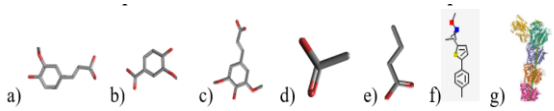

Figure 5. Chemical structures of candidate ligands and the STMN1 target protein prepared for docking analysis, a) Ferulic Acid; b) Protocatechuic Acid; c) Sinapic Acid; d) Acetic Acid; e) Butanoic Acid; f) 3-[2-(N-methylaminomethyl)phenylthio]phenol; g) Protein stathmin.

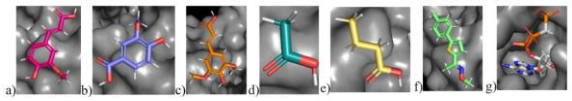

Figure 6. Molecular docking visualization of phosphorylated STMN1 (stathmin): 3D structure of the stathmin–phosphate complex

Candidate ligands for molecular docking against STMN1 (stathmin) were curated from Dr. Duke's Phytochemical and Ethnobotanical Database and matched with 3D structures from PubChem prior to docking simulations to evaluate binding affinity and identify interacting residues (Duke, 2016; Trott & Olson, 2010). A phosphate group was incorporated into the STMN1 model because STMN1 is regulated by phosphorylation, and phosphorylation at key serine residues is known to modulate stathmin's microtubule-related activity in cancer-relevant

contexts (Liu et al., 2023). The ligand collection and the STMN1 model are illustrated in Figure 5, whereas the docked poses within the binding pocket and their interaction representations together with the phosphorylated STMN1 visualization are shown in Figure 6.

Docking analysis showed that the control ligand GDP exhibited the strongest binding affinity (−10.6 kcal/mol), whereas among the tested compounds, sinapic acid (−7.5 kcal/mol) and ferulic acid (−7.4 kcal/mol) demonstrated higher affinities than protocatechuic acid (−6.6

Table 1. STMN1–ligand interaction map derived from docking and LigPlot+ analysis: key residues, functional groups, and contact distances

Substances	Binding affinity (kcal/mol)	Binding distance (A^0)	Amino acid and the bound funct. groups	2D binding depiction
GDP Ligand control	-10.6	2,78 2,61 2,89 2,75 3,28 3,11 3,26 3,06 2,96 2,86 2,84 2,76 2,84 2,68	TYR222: H-O ASN226: H-O ASN226: H-O ASN204: H-O ASN204: H-O VALL75: alkyl SER138: H-O SER138: H-O SER138: H-O CYS12: H-O GLY144: H-O GLN11: H-O GLY142: H-O THR143:H-O	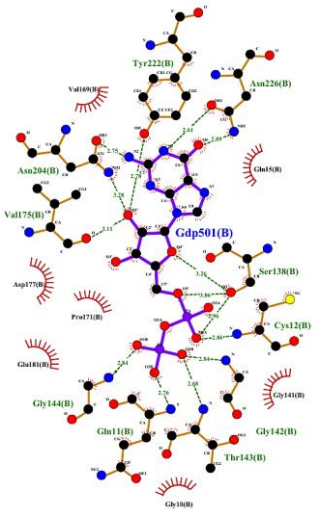
Ferulic Acid	-7.4	2,97 3,03 3,08 3,22 3,11 3,09 2,88 3,01	GLN11: H-O CYS12: H-O GLY13: C-H SER138: H-O ALA9: alkyl ASN204: H-O GLY142: C-H THR143: H-O	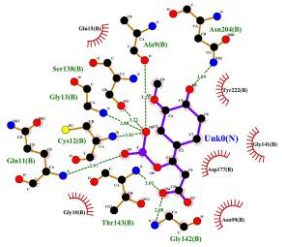
Sinapic Acid	-7.5	2,75 3,11 3,20 3,18 3,17 2,71 3,01	ASN99: H-O THR143: H-O GLY142: C-H GLY142: C-H SER138: H-O SER138: H-O SER145: C-H	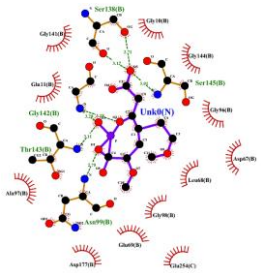
Protocatechuic Acid	-6.6	2,57 3,16 3,03 2,78 3,05 3,20 3,19 2,98 2,80 2,92	GLY142: C-H GLY142: C-H ASN99: H-O ASN99: H-O ASN99: H-O SER138: H-O THR143: H-O THR143:H-O THR143: H-O GLY144: C–H	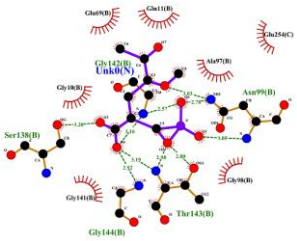

kcal/mol) (Table 1). Recurrent interactions involving residues such as GLN11, CYS12, SER138, GLY142, and THR143 suggested a relatively conserved binding region within STMN1 (Zeng et al., 2024). Overall, sinapic acid and ferulic acid emerged as the most promising candidate ligands, although their predicted binding affinities remained lower than that of the control ligand GDP (Papagiouvannis et al., 2024; Theodosis-Nobelos et al., 2023)

Macrophage isolation and culture observations

Peritoneal macrophages isolated from BALB/c mice produced a cell suspension suitable for microscopy-based analysis. The coverslip preparation provided a denser and more clearly distinguishable cell distribution than the non-coverslip condition (Figure 7). Hemocytometer counting showed a cell density of 1.89×10^6 cells/mL, confirming that the isolated cells were adequate for subsequent morphological observation and the latex-bead phagocytosis assay(Green & Sambrook, 2019).

(a) (b)

Figure 7. Results of isolation of peritoneal cavity macrophage cells from BALB/c mice (Mus musculus) without coverslip (a) and with coverslip (b).

Macrophage isolation and culture observation

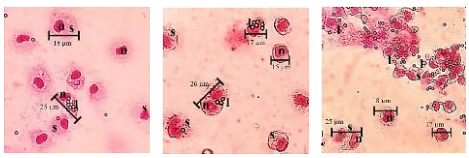

(a) (b) (c)

Figure 8. Morphology of macrophage cells treated with 0 µL (a), 5 µL (b), and 10 µL (c). Note: (n) nucleus, (s) cytoplasm, (l) latex beads (400× magnification).

Microscopic examination of 10% Giemsa-stained macrophages at 400× magnification clearly distinguished the nuclei and cytoplasm, enabling reliable cell identification (Velez-Hoyos & Jimenez-tobon, 2022). Representative micrographs (Figure 8) showed a dose-dependent increase in latex bead uptake, with the highest bead density observed in the 10 µL group. The observed cell size (approximately 15–26 µm) was consistent with the typical morphology of macrophages (Fakoya et al., 2025).

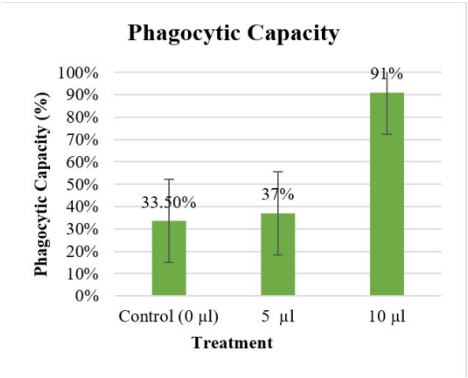

Figure 9. Diagram of phagocytic capacity.

Table 2. Results of the Games–Howell post hoc test on phagocytic capacity.

Concentration (µL/mL)	Compared with (µL/mL)	Mean Difference	Sig.	p (α = 0.05)
0	5	−3.33	0.143	< 0.05
	10	−56.00*	<0.001	< 0.05
5	0	3.33	0.143	< 0.05
	10	−52.66*	<0.001	< 0.05
10	0	56.00*	<0.001	< 0.05
	5	52.66*	<0.001	< 0.05

Phagocytic capacity of macrophages

Phagocytic capacity differed among treatment groups. The control (0 µL), 5 µL, and 10 µL groups exhibited phagocytic capacities of 33.5%, 37%, and 91%, respectively (Figure 9). Games–Howell analysis showed no significant difference between the 0 and 5 µL groups ($p = 0.143$), whereas significant differences were observed between the 0 and 10 µL groups and between the 5 and 10 µL groups (both $p < 0.001$) (Table 2).

Macrophage phagocytosis assay observations

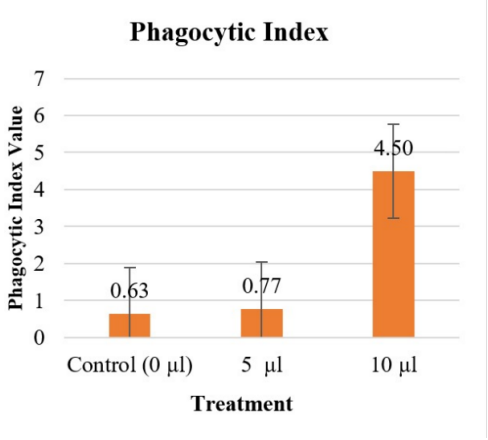

Figure 10. Diagram of the macrophage phagocytic index.

Table 3. Results of the Games–Howell post hoc test on the phagocytic index.

Concentration (µl/mL)		Mean Difference	Sig.	P	Conclusion
0	5	-0,191*	0,044	< 0,05	Significant
	10	-3,080*	0,016		
5	0	0,191*	0,044		
	10	-2,888*	0,020		
10	0	3,080*	0,016		
	5	2,888*	0,020		

The macrophage phagocytic index exhibited a sharper change than phagocytic capacity, capturing not only "how many cells are active" but also "how intensively" the participating cells internalize particles. The macrophage phagocytic index increased from 0.63 in the control group (0 µL) to 0.77 at 5 µL and rose markedly to 4.50 at 10 µL (Figure 10), indicating a dose-dependent enhancement in phagocytic activity. Games–Howell post hoc analysis confirmed significant differences among all treatment groups ($p < 0.05$) (Table 3). Although the 5 µL treatment produced only a modest increase, the 10 µL dose resulted in a substantially greater enhancement of phagocytic activity.

DISCUSSION

In silico prediction of STMN1 interaction by shallot-derived candidate ligands

Candidate ligands curated from phytochemical databases and literature sources were docked to STMN1, and the resulting binding affinities and interaction profiles were evaluated as a first-pass in silico screen of predicted STMN1 interaction (Trott & Olson, 2010). Docking outcomes showed that the GDP control ligand produced the strongest predicted affinity (−10.6 kcal/mol) and formed multiple short-range contacts within the binding pocket, serving as a benchmark for comparison (Table 1). Among the tested phenolic acids, sinapic acid (−7.5 kcal/mol) and ferulic acid (−7.4 kcal/mol) showed the most favorable predicted binding affinities, whereas protocatechuic acid (−6.6 kcal/mol) showed weaker predicted binding (Table 1). Although the candidate ligands did not surpass the control, the affinity ordering suggests a possible trend in which substituted phenolic acids with more extensive functionalization may show more favorable predicted interactions within the STMN1 pocket under the present docking conditions (Zeng et al., 2024).

Interaction mapping further supports this ranking by highlighting recurring residues and plausible contact chemistry. Several residues appeared repeatedly across ligand–STMN1 complexes (e.g., SER138, GLY142, THR143, and GLN11/CYS12), suggesting that multiple ligands may occupy a relatively consistent predicted binding region of STMN1 (Table 1). Collectively, the docking results indicate that sinapic acid and ferulic acid showed the most favorable predicted interactions among the tested candidates and therefore represent the strongest in silico candidates for further STMN1-oriented evaluation in this study. At the same time, docking remains a predictive approach; recent evaluations emphasize that scoring functions and sampling limitations require cautious interpretation and that experimental validation is needed before concluding biochemical inhibition (Agu et al., 2023).

In vitro macrophage functional response to NLC treatment

In vitro testing was conducted to evaluate whether the synthesized NLC dispersion could modulate macrophage phagocytosis as an early functional readout related to innate immune response in the tumor microenvironment. Peritoneal macrophages isolated from BALB/c mice produced a cell suspension suitable for microscopy-based assays, and the coverslip preparation enabled clearer observation than the non-coverslip condition (Figure 7) (De Jesus et al., 2022; Khatua et al., 2022). Giemsa-stained micrographs showed distinguishable nuclei and cytoplasm, as well as latex beads associated with macrophages across treatment groups, supporting the feasibility of quantitative phagocytosis analysis (Figure 8) (De Jesus et al., 2022).

The biological response should be considered in relation to the physicochemical characteristics of the synthesized NLC system. Visual observation showed differences between homogenized and non-homogenized preparations (Figure 1), while PSA/DLS analysis indicated particle-size variation and moderate dispersity (Figure 2 and Figure 3). SEM observation also revealed irregular particulate structures with aggregation tendency (Figure 4). These findings suggest that the NLC system delivered to macrophages consisted of lipid-based particulate entities whose dispersion state may influence cell-particle interaction, membrane contact, and bead uptake response.

Quantitative analysis showed that the 10 µL treatment produced the strongest enhancement of macrophage phagocytic activity. Phagocytic capacity increased from 33.5% (0 µL) to 37% (5 µL) and 91% (10 µL), with significant differences between 10 µL and both lower groups ($p < 0.001$), while the 0 µL and 5 µL groups did not differ significantly (Table 2). The phagocytic index also increased from 0.63 to 0.77 and 4.50, respectively, with all pairwise comparisons showing significant differences ($p < 0.05$) (Table 3). These results indicate that the 10 µL NLC treatment increased both the proportion of active macrophages and the intensity of bead internalization, providing evidence of enhanced macrophage functional activity (Riezk et al., 2025; Ueno et al., 2021).

However, these findings should not be interpreted as direct evidence of anti-metastatic activity or M2 macrophage inhibition, since macrophage polarization markers such as CD206, CD163, Arg-1, IL-10, iNOS, and CD86 were not assessed. Further studies using marker-based assays and macrophage-cancer cell co-culture or migration assays are required to confirm phenotype-specific and anti-metastatic relevance (Lim et al., 2024; Jeitler et al., 2024).

CONCLUSIONS

Shallot leaf extract was formulated into an NLC dispersion using an emulsification–ultrasonication approach. PSA/DLS and SEM findings indicated the presence of particulate structures. In silico docking against STMN1 identified sinapic acid and ferulic acid as the best-ranked phenolic candidates among the tested ligands. Macrophage testing showed that the 10 µL dose produced the strongest enhancement of phagocytic capacity and phagocytic index under the present latex-bead assay conditions. Further studies involving macrophage polarization markers are required to validate the formulation stability and biological relevance of the synthesized NLC dispersion.

ACKNOWLEDGMENT

The authors have no acknowledgments.

AUTHORS' CONTRIBUTIONS

Amna Falistina (A.F.): Investigation; Data curation; Writing—original draft.
Bilqis Alfisyahani (B.A.): Investigation; Formal analysis; Visualization; Writing—original draft.
Yuda Faturohman (Y.F.): Conceptualization; Methodology; Formal analysis; Software; Supervision; Project administration; Writing—review & editing.
Adyatma Riyandino (A.R.): Methodology; Writing—review & editing.
Anantazea Deniss Kumara (A.D.K.): Supervision; Writing—review & editing.
Talitha Widiatningrum (T.W.): Conceptualization; Investigation (laboratory work)**;** Supervision; Writing—review & editing.

CONFLICT OF INTERESTS

Authors declare no conflict of interest.

ETHICAL CONSIDEATION

Ethical approval was not required for this study.

BIBLIOGRAPHY

Agu, P. C., Afiukwa, C. A., Orji, O. U., Ezeh, E. M., Ofoke, I. H., Ogbu, C. O., Ugwuja, E. I., & Aja, P. M. (2023). Molecular docking as a tool for the discovery of molecular targets of nutraceuticals in diseases management. *Sci. Rep.*, *13*(1), 13398.

Bray, F., Laversanne, M., Sung, H., Ferlay, J., Siegel, R. L., Soerjomataram, I., & Jemal, A. (2024). *Global cancer statistics 2022: GLOBOCAN estimates of incidence and mortality worldwide for 36 cancers in 185 countries*. *3*(74). https://doi.org/10.3322/caac.21834

Bresch, H., Hodoroaba, V.-D., Schmidt Alexandra and Rasmussen, K., & Rauscher, H. (2022). Counting small particles in electron microscopy images-proposal for rules and their application in practice. *Nanomaterials (Basel)*, *12*(13), 2238.

Calderon-Jacinto, R., Matricardi, P., Gueguen, V., Pavon-Djavid, G., Pauthe, E., & Rodriguez-Ruiz, V. (2022). Dual Nanostructured Lipid Carriers/Hydrogel System for Delivery of Curcumin for Topical Skin Applications. *Biomolecules*, *12*(6).

Chauhan, I., Yasir, M., Verma, M., & Singh, A. P. (2020). Nanostructured lipid carriers: A groundbreaking approach for transdermal drug delivery. *Adv. Pharm. Bull.*, *10*(2), 150–165.

De Jesus, A., Pusec, C. M., Nguyen, T., Keyhani-Nejad, F., Gao, P., Weinberg, S. E., & Ardehali, H. (2022). Optimized protocol to isolate primary mouse peritoneal macrophage metabolites. *STAR Protoc.*, *3*(4), 101668.

Duke, J. A. (2016). *Dr. Duke's phytochemical and ethnobotanical databases*. Ag Data Commons.

Elkhateeb, O., Badawy, M. E. I., Tohamy, H. G., Abou-Ahmed, H., El-Kammar, M., & Elkhenany, H. (2023). Curcumin-infused nanostructured lipid carriers: a promising strategy for enhancing skin regeneration and combating microbial infection. *BMC Vet. Res.*, *19*(1), 206.

Fakoya, A. O., Naeem, A., & Pierre, L. (2025). Histology, alveolar macrophages. In *StatPearls*. StatPearls Publishing.

Friedman-DeLuca, M., Karagiannis, G. S., Condeelis, J. S., Oktay, M. H., & Entenberg, D. (2024). Macrophages in tumor cell migration and metastasis. *Frontiers in Immunology*, *Volume 15-2024*. https://doi.org/10.3389/fimmu.2024.1494462

Green, M. R., & Sambrook, J. (2019). Estimation of cell number by hemocytometry counting. *Cold Spring Harb. Protoc.*, *2019*(11), db.prot097980.

Hackley, V., & Clogston, J. (2020). *NIST - NCL Joint Assay Protocol, PCC-1*. NCIP Hub.

Imran, M., Iqubal, M. K., Imtiyaz Khalid and Saleem, S., Mittal, S., Rizvi M Moshahid A and Ali, J., & Baboota, S. (2020). Topical nanostructured lipid carrier gel of quercetin and resveratrol: Formulation, optimization, in vitro and ex vivo study for the treatment of skin cancer. *Int. J. Pharm.*, *587*(119705), 119705.

Iwar, K., Ochar, K., Seo, Y. A., Ha, B.-K., & Kim, S.-H. (2024). Alliums as potential antioxidants and anticancer agents. *Int. J. Mol. Sci.*, *25*(15), 8079.

Jeitler, R., Glader, C., König, G., Kaplan, J., Tetyczka, C., Remmelgas, J., Mußbacher, M., Fröhlich, E., & Roblegg, E. (2024). On the Structure, Stability, and Cell Uptake of Nanostructured Lipid Carriers for Drug Delivery. *Molecular Pharmaceutics*, *21*(7), 3674–3683. https://doi.org/10.1021/acs.molpharmaceut.4c00392

Khatua, S., Simal-Gandara, J., & Acharya, K. (2022). Understanding immune-modulatory efficacy in vitro. *Chem. Biol. Interact.*, *352*(109776), 109776.

Kim, S., Chen, J., Cheng, T., Gindulyte, A., He, J., He, S., Li, Q., Shoemaker, B. A., Thiessen, P. A., Yu, B., Zaslavsky Leonid and Zhang, J., & Bolton, E. E. (2023). PubChem 2023 update. *Nucleic Acids Res.*, *51*(D1), D1373–D1380.

Krakowska-Sieprawska, A., Kiełbasa, A., Rafińska, K., Ligor, M., & Buszewski, B. (2022). Modern methods of pre-treatment of plant material for the extraction of bioactive compounds. *Molecules*, *27*(3), 730.

Kumari, M., Gohil, D., & Sadhu, P. (2026). Nanostructured lipid carriers for topical drug delivery: A comprehensive review of design, mechanisms, and therapeutic advances. *Next Nanotechnology*, *9*, 100367. https://doi.org/10.1016/j.nxnano.2026.100367

Lim, S. H., Wong, T. W., & Tay, W. X. (2024). Overcoming colloidal nanoparticle aggregation in biological milieu for cancer therapeutic delivery: Perspectives of materials and particle design. *Advances in Colloid and Interface Science*, *325*, 103094. https://doi.org/https://doi.org/10.1016/j.cis.2024.103094

Liu, R., Liang, X., Guo, H., Li, S., Yao, W., Dong, C., Wu, J., Lu, Y., Tang, J., & Zhang, H. (2023). STNM1 in human cancers: role, function and potential therapy sensitizer. *Cellular Signalling*, *109*, 110775. https://doi.org/https://doi.org/10.1016/j.cellsig.2023.110775

Papagiouvannis, G., Theodosis-Nobelos, P., & Rekka, E. A. (2024). Trolox, Ferulic, Sinapic, and Cinnamic Acid Derivatives of Proline and GABA with Antioxidant and/or Anti-Inflammatory Properties. *Molecules*, *29*(16). https://doi.org/10.3390/molecules29163763

Pavlova, E., Shaposhnikova, D., Petrichuk, S., Radygina, T., & Erokhina, M. (2023). Quantitative analysis of latex beads phagocytosis by human macrophages using imaging flow cytometry with extended depth of field (EDF). *Methods Mol. Biol.*, *2635*, 203–215.

Riezk, A., O'Keeffe, A., Van Bocxlaer, K., Yardley, V., & Croft, S. L. (2025). Comparative assessment of macrophage responses and antileishmanial efficacy in dynamic vs. Static culture systems utilizing chitosan-based formulations. *PLOS ONE*, *20*(3), e0319610-. https://doi.org/10.1371/journal.pone.0319610

Theodosis-Nobelos, P., Papagiouvannis, G., & Rekka, E. A. (2023). Ferulic, Sinapic, 3,4-Dimethoxycinnamic Acid and Indomethacin Derivatives with Antioxidant, Anti-Inflammatory and Hypolipidemic Functionality. *Antioxidants*, *12*(7). https://doi.org/10.3390/antiox12071436

Trott, O., & Olson, A. J. (2010). AutoDock Vina: improving the speed and accuracy of docking with a new scoring function, efficient optimization, and multithreading. *J. Comput. Chem.*, *31*(2), 455–461.

Ueno, T., Yamamoto, Y., & Kawasaki, K. (2021). Phagocytosis of microparticles increases responsiveness of macrophage-like cell lines U937 and THP-1 to bacterial lipopolysaccharide and lipopeptide. *Scientific Reports*, *11*(1), 6782. https://doi.org/10.1038/s41598-021-86202-5

Varadi, M., Anyango, S., Deshpande, M., Nair, S., Natassia, C., Yordanova, G., Yuan, D., Stroe, O., Wood, G., Laydon, A., Žídek, A., Green, T., Tunyasuvunakool, K., Petersen, S., Jumper, J., Clancy, E., Green, R., Vora, A., Lutfi, M., … Velankar, S. (2022). AlphaFold Protein Structure Database: massively expanding the structural coverage of protein-sequence space with high-accuracy models. *Nucleic Acids Research*, *50*(D1), D439–D444. https://doi.org/10.1093/nar/gkab1061

Velez-Hoyos, A., & Jimenez-tobon, G. A. (2022). Highlights of infectious agents in tissue. *Pathology*, *54*(2), 217–224. https://doi.org/https://doi.org/10.1016/j.pathol.2021.10.004

Zeng, L., Lyu, X., Yuan, J., Chen, Y., Wen, H., Zhang, L., Shi, J., Liu, B., Li, W., & Yang, S. (2024). STMN1 promotes tumor metastasis in non-small cell lung cancer through microtubule-dependent and nonmicrotubule-dependent pathways. *Int. J. Biol. Sci.*, *20*(4), 1509–1527.